〈Technical Note〉

A PARTICLE TRACKING MODEL TO PREDICT THE DEBRIS TRANSPORT ON THE CONTAINMENT FLOOR

YOUNG SEOK BANG*, GIL SOO LEE, BYUNG-GIL HUH, DEOG-YEON OH and SWENG-WOONG WOO
Korea Institute of Nuclear Safety
P.O.Box 114, Yuseong, Daejeon, Republic of Korea, 305-335
*Corresponding author. E-mail : k164bys@kins.re.kr

Received September 1, 2009
Accepted for Publication January 28, 2010

An analysis model on debris transport in the containment floor of pressurized water reactors is developed in which the flow field is calculated by Eulerian conservation equations of mass and momentum and the debris particles are traced by Lagrange equations of motion using the pre-determined flow field data. For the flow field calculation, two-dimensional Shallow Water Equations derived from Navier Stokes equations are solved using the Finite Volume Method, and the Harten-Lax-van Leer scheme is used for accuracy to capture the dry-to-wet interface. For the debris tracing, a simplified two-dimensional Lagrangian particle tracking model including drag force is developed. Advanced schemes to find the positions of particles over the containment floor and to determine the position of particles reflected from the solid wall are implemented. The present model is applied to calculate the transport fraction to the Hold-up Volume Tank in Advanced Power Reactors 1400. By the present model, the debris transport fraction is predicted, and the effect of particle density and particle size on transport is investigated.

KEYWORDS : Debris Transport, Largrangian Particle Tracking, Containment Floor, APR1400

1. INTRODUCTION

Following a loss-of-coolant accident (LOCA), debris generated by LOCA may run into the containment floor and to sump, block the sump screen (or strainer), increase the hydraulic head loss across the screen, and, eventually, have an adverse effect on the long-term recirculation cooling operation in the pressurized water reactor (PWR) (Generic Safety Issue 191) [1]. The head loss can be further increased by the product generated by chemical reactions of insulation material such as calcium silicate with the spray buffer agent or metallic material such as aluminum with borated water [2]. By this issue, the replacement of the containment recirculation sump strainer is expected for the most of domestic operating nuclear power plants (NPP) having a limited strainer area [3].

In the design of a new strainer, the minimum screen area which can incorporate the potential debris loading is the most important factor. The minimum screen area has been determined using transport fraction (TF) defined by the ratio of the amount of debris accumulated on the screen to the amount of debris generated by a LOCA. Since TF is strongly dependent on the geometric configuration within the containment and thermal-hydraulic behavior including containment spray, a reasonable determination of TF considering the plant specific condition and hydraulic analysis has been emphasized [4].

The debris transport mechanism in PWR can be divided into three phases: blowdown, washdown, and pool recirculation. For the existing PWR, TF was determined in a phase-averaged sense through simple analysis and experiments [5]. However, the division cannot be applied to some NPP, such as an Advanced Power Reactor 1400 (APR1400) [6], having no recirculation operation. Transport of debris to sump in APR1400 is initiated from the early phase of a LOCA. This implies that the calculation should be done in a fully transient manner and that the effects of blowdown and washdown should be implemented into the pool transport analysis.

The present study is to examine an analysis model on debris transport in a containment pool in a transient manner. For this purpose, the flow field is calculated by the Eulerian conservation equations of mass and momentum and the debris particle is traced by the Lagrange equation of motion using the flow field data, i.e., Euler-Lagrange scheme. The method generally requires (1) a hydraulic solver to determine a time-dependent fluid velocity, (2) a debris tracing model considering the physical properties such as configuration, size, and density of debris, and (3) consideration of the change of the velocity field by the interactions of debris-fluid and debris-debris.

Solver of the flow field on the containment floor should

address several physical phenomena including the strong water jet from the break, the impingement water flow to the structural wall, the water spreading over the dry floor, the surface waves and reflective waves over the floor, etc. A capability to describe the complex geometry of containment and an accurate numerical scheme to capture the sharp interface between the dry floor and the wet floor are required for the hydraulic solver. The calculation should also be carried out with a practical computational time and practical number of meshes for the calculation domain such as a containment floor with an inner diameter of 40 m. Commercial computational fluid dynamic (CFD) codes may be used; however, it is still difficult to get a transient solution even in the short term due to the high computation time [7]. Recently, a flow field calculation solver suitable for those requirements was developed by the present authors [8]. The method was to solve two-dimensional Shallow Water Equations (SWE) [9] derived from Navier-Stokes equations using the Finite Volume Method (FVM). For the accuracy to capture the dry-to-wet interface, the Harten-Lax-van Leer (HLL) scheme [10] was adopted in the present model.

For debris tracing, a simplified two-dimensional Lagrangian particle tracking model was developed. To find the positions of particles over the containment floor, a scheme of Martin et al. [11] was used while a scheme of Haselbacher et al. [12] was adopted to determine the reflected positions from the solid wall. Generally, LOCA-generated debris includes fibers and particles with various configurations and sizes. However, it is impractical to develop a model incorporating all those aspects under the current status of technology. Instead, the spherical shape of particle was assumed to represent the debris. And the interactions of debris-fluid and debris-debris were neglected to eliminate a reduction of debris velocity from a conservative viewpoint [13,14].

The model was applied to preliminarily calculate the transport fraction to the Hold-up Volume Tank (HVT), which is a unique flow path to the containment sump in APR1400.

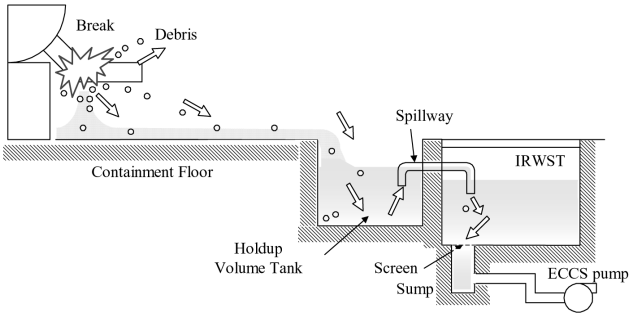

Fig. 1. Description of Debris Transport

2. CALCULATION MODEL

2.1 Shallow Water Equation Solver

A two-dimensional shallow water equations (SWE) can be obtained from the Navier-Stokes equation by assuming zero vertical velocity:

$$\frac{\partial \boldsymbol{U}}{\partial t}+\frac{\partial \boldsymbol{F}}{\partial x}+\frac{\partial \boldsymbol{G}}{\partial y}=\frac{\partial \boldsymbol{R}_x}{\partial x}+\frac{\partial \boldsymbol{R}_y}{\partial y}+\boldsymbol{S} \tag{1}$$

$$\boldsymbol{U}=\begin{bmatrix} h \\ hu \\ hv \end{bmatrix},\ \boldsymbol{F}=\begin{bmatrix} hu \\ hu^2+1/2gh^2 \\ huv \end{bmatrix},\ \boldsymbol{G}=\begin{bmatrix} hv \\ huv \\ hv^2+1/2gh^2 \end{bmatrix} \tag{2a}$$

$$\boldsymbol{R}_x=\begin{bmatrix} 0 \\ \nu_e(\partial hu/\partial x) \\ \nu_e(\partial hv/\partial x) \end{bmatrix},\ \boldsymbol{R}_y=\begin{bmatrix} 0 \\ \nu_e(\partial hu/\partial y) \\ \nu_e(\partial hv/\partial y) \end{bmatrix},\ \boldsymbol{S}=\begin{bmatrix} B(t) \\ gh(S_{ox}-S_{fx}) \\ gh(S_{oy}-S_{fy}) \end{bmatrix} \tag{2b}$$

$$S_{ox}=-\frac{\partial z_b}{\partial x},\ S_{oy}=-\frac{\partial z_b}{\partial y} \tag{2c}$$

$$S_{fx}=\frac{un_m{}^2\sqrt{u^2+v^2}}{h^{4/3}},\ S_{fy}=\frac{vn_m{}^2\sqrt{u^2+v^2}}{h^{4/3}}, \tag{2d}$$

where h, u, v, and z_b denote the water level from the bed, velocity components in x and y directions, and bed elevation, respectively. And n_m, $B(t)$, and ν_e are the Manning bed friction coefficient ($m^{-1/3}s$), water source term into the flow field, and depth-averaged effective viscosity, respectively. The bed slope (S_o), and the momentum lost by friction with a bed (S_f) of water, are also included. A detailed description of the SWE can be found in [8].

The integration of Eq. (1) over area A surrounded by a closed path C can be written as Eq. (3), and the fully explicit numerical form of Eq. (3) for the triangular cell can be written as Eq. (4):

$$\int_A \frac{\partial \boldsymbol{U}}{\partial t}dA+\int_C(\boldsymbol{F}n_x+\boldsymbol{G}n_y)dC=\int_C(\boldsymbol{R}_x n_x+\boldsymbol{R}_y n_y)dC+\int_A \boldsymbol{S}dA \tag{3}$$

$$\boldsymbol{U}_k^{n+\frac{1}{2}}=\boldsymbol{U}_k^n-\frac{\Delta t}{2A_k}\sum_{j=1}^{3}\left[(\boldsymbol{F}_{kj}^n n_{xj}+\boldsymbol{G}_{kj}^n n_{yj})-(\boldsymbol{R}_{xkj}^n n_{xj}+\boldsymbol{R}_{ykj}^n n_{yj})\right]L_j+\boldsymbol{S}_k{}^n\frac{\Delta t}{2} \tag{4a}$$

$$\boldsymbol{U}_k^{n+1}=\boldsymbol{U}_k^{n+\frac{1}{2}}-\frac{\Delta t}{2A_k}\sum_{j=1}^{3}\{(\boldsymbol{F}^{HLL}{}_{kj}^{n+\frac{1}{2}}n_{xj}+\boldsymbol{G}^{HLL}{}_{kj}^{n+\frac{1}{2}}n_{yj}) -(\boldsymbol{R}_{xkj}^{n+\frac{1}{2}}n_{xj}+\boldsymbol{R}_{ykj}^{n+\frac{1}{2}}n_{yj})\}L_j+\boldsymbol{S}_k^{n+\frac{1}{2}}\frac{\Delta t}{2} \tag{4b}$$

In this expression, the predictor-corrector method was applied to reserve the second order accuracy in time. The flux term in Eq. (4a) can be calculated in a normal central difference scheme in the predictor step. However, this calculation leads to an unphysical oscillation and instability of the solution, especially at the wet-dry interface.

Thus, the Harten-Lax-van Leer scheme was applied in the corrector step as follows:

$$\boldsymbol{F}^{HLL}=\begin{cases}\boldsymbol{F}(\boldsymbol{U}_L) & if \quad s_L>0\\ \left[(s_R\boldsymbol{F}(\boldsymbol{U}_L)-s_L\boldsymbol{F}(\boldsymbol{U}_R))\cdot\boldsymbol{n}\right. & \\ \left.\quad +s_Ls_R(\boldsymbol{U}_R-\boldsymbol{U}_L)\right]/(s_R-s_L) & if \quad s_L\le 0\le s_R\\ \boldsymbol{F}(\boldsymbol{U}_R) & if \quad s_R>0\end{cases} \tag{5}$$

$$\begin{Bmatrix}s_L\\ s_R\end{Bmatrix}=\begin{Bmatrix}\min(\boldsymbol{V}_L\cdot\boldsymbol{n}-\sqrt{gh_L},\ \boldsymbol{V}^*\cdot\boldsymbol{n}-c^*)\\ \max(\boldsymbol{V}_R\cdot\boldsymbol{n}-\sqrt{gh_R},\ \boldsymbol{V}^*\cdot\boldsymbol{n}+c^*\end{Bmatrix}, \tag{6}$$

where, velocity vector, $\boldsymbol{V}=u\boldsymbol{i}+v\boldsymbol{j}$. The asterisked variables, $\boldsymbol{V}^*$ and c^*, are defined as follows:

$$\begin{aligned}\boldsymbol{V}^*\cdot\boldsymbol{n}\mp c^*=&\left[\frac{1}{2}(\boldsymbol{V}_L+\boldsymbol{V}_R)\cdot\boldsymbol{n}+\sqrt{gh_L}-\sqrt{gh_R}\right]\\ &\mp\left[\frac{1}{4}(\boldsymbol{V}_L-\boldsymbol{V}_R))\cdot\boldsymbol{n}+\frac{1}{2}(\sqrt{gh_L}+\sqrt{gh_R})\right],\end{aligned} \tag{7}$$

where subscripts L and R represent the values at the cell to the left of the interface and to the right of the cell, respectively. s_R and s_L mean the wave speeds at those cells. The detailed description of the numerical scheme and boundary conditions can be found in [8].

2.2 Particle Tracking Model

Following a LOCA, debris particles may be transported through collisions with other particles, sinking and rising due to buoyant force, and settling-down due to low velocity. The present model did not consider those aspects, which can be unrealistic but conservative from the viewpoint of debris transport. Therefore, the debris transport fraction is be determined by considering the drag force and geometric effect.

The position of a particle i at time $n+1$ in two-dimensional Cartesian coordinates can be calculated from the position at n time level and movement during time interval Δt_p as follows:

$$\boldsymbol{x}_i^{n+1}=x_i^{n+1}\boldsymbol{i}+y_i^{n+1}\boldsymbol{j}=\boldsymbol{x}_i^n+\boldsymbol{w}_i^n\Delta t_P \tag{8}$$

where particle velocity, $\boldsymbol{w}_i=u_i\boldsymbol{i}+v_i\boldsymbol{j}$, can be solved from the equation of motion with fluid velocity ($\boldsymbol{V}_f=u_f\boldsymbol{i}+v_f\boldsymbol{j}$) which was already determined by the SWE solver,

$$m_i\frac{d\boldsymbol{w}_i}{dt}=-\boldsymbol{D}_i=-A_iC_D\frac{1}{2}\rho_f\left|\boldsymbol{w}_i-\boldsymbol{V}_f\right|(\boldsymbol{w}_i-\boldsymbol{V}_f) \tag{9}$$

Assuming the particle is in a spherical shape with diameter d_i and density ρ_i, and expressing the time derivative term in an explicit manner,

$$\boldsymbol{w}_i^n=\boldsymbol{w}_i^{n-1}-\frac{3}{4}\frac{\rho_f\Delta t_p}{\rho_i d_i}C_D^{n-1}\left|\boldsymbol{w}_i^{n-1}-\boldsymbol{V}_f^{n-1}\right|(\boldsymbol{w}_i^{n-1}-\boldsymbol{V}_f^{n-1}) \tag{10}$$

The drag coefficient, C_D, can be expressed by the Schiller and Neumann correlation [14]:

$$C_D=\begin{cases}24/\mathrm{Re} & for\ \ Re<0.1\\ Max\left[24/\mathrm{Re}(1+0.15\,\mathrm{Re}^{0.687}),\ 0.44\right] & for\ \ 0.1<Re<1000\\ 0.44 & for\ \ 1000<Re<1.2\times10^5\end{cases} \tag{11}$$

where Reynolds number is defined as follows:

$$\mathrm{Re}=\frac{\rho_f\left|\boldsymbol{w}_i^n-\boldsymbol{V}_f^n\right|d_i}{\mu_f} \tag{12}$$

To define the fluid velocity, the cell having the particle, i.e., the hosting cell, must be identified. To save the time required to search for the hosting cell, the method proposed by Martin [11] was introduced. If the particle is located within the cell, then the following conditions should be met (Fig. 2(a)).

$$\begin{aligned}E_1&=\boldsymbol{n}_1\cdot(\boldsymbol{p}_i-\boldsymbol{m}_1)<0\\ E_2&=\boldsymbol{n}_2\cdot(\boldsymbol{p}_i-\boldsymbol{m}_2)<0\\ E_3&=\boldsymbol{n}_3\cdot(\boldsymbol{p}_i-\boldsymbol{m}_3)<0\end{aligned} \tag{13}$$

where $\boldsymbol{m}_1$, $\boldsymbol{m}_2$, $\boldsymbol{m}_3$, and $\boldsymbol{n}_1$, $\boldsymbol{n}_2$, $\boldsymbol{n}_3$ denote vectors to the centroids and unit normal vectors of three sides of the triangle and $\boldsymbol{p}_i$ is a particle position vector, respectively. If those conditions are not met, the particle will be outside the cell k. In such a case, the adjacent cell sharing side j with cell k and having a maximum value of E_j will be searched first.

An intersection of a particle trajectory with a side of a cell can be determined as follows (Fig.2(b)). Consider the particle moves from position $\boldsymbol{p}$ to position $\boldsymbol{q}$ by intersecting with the side at position $\boldsymbol{r}$. Assuming $\boldsymbol{t}$ is a unit vector from $\boldsymbol{p}$ to $\boldsymbol{q}$, $\boldsymbol{C}$ is a center of the side, and vector $\boldsymbol{r}-\boldsymbol{p}=\alpha\,\boldsymbol{t}$, then

$$(\boldsymbol{r}(\alpha)-\boldsymbol{C})\cdot\boldsymbol{n}=0 \tag{14}$$

From those equations, α can be determined as follows:

$$\alpha=\frac{(\boldsymbol{C}-\boldsymbol{p})\cdot\boldsymbol{n}}{(\boldsymbol{t}\cdot\boldsymbol{n})} \tag{15}$$

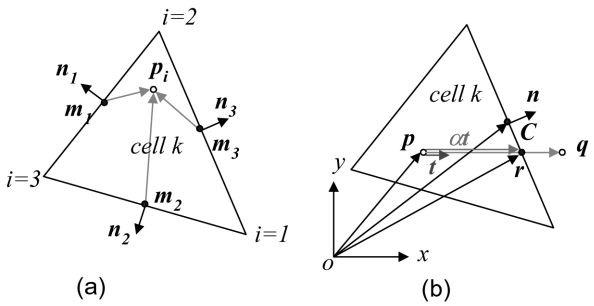

Fig. 2. Host Cell Criteria and Intersection of Particle Trajectory

Let the distance from $\boldsymbol{p}$ to $\boldsymbol{q}$ be d, and $\alpha > d$ means position $\boldsymbol{q}$ is inside the cell.

If the intersecting side is a reflective boundary, i.e., solid wall, the reflection of the particle should be considered (Fig. 3). From the vector operation, the new position $\boldsymbol{q}'$ can be determined as follows:

$$\boldsymbol{q}' = \boldsymbol{q} - 2\{(\boldsymbol{q} - \boldsymbol{r}) \cdot \boldsymbol{n}\}\boldsymbol{n} \tag{16}$$

The sequence of calculation is as follows:

(1) For the given mesh system, input the transient velocities at each cell, the total number of particles, and the physical properties. Positions of particles are determined to be randomly distributed. The particle hosting cells are determined by Eq. (13). Initial velocities of the particles are set to zero.
(2) The time step is increased, and the fluid velocity of each hosting cell is determined by interpolation from the fluid velocity data. Reynolds number, drag force, and particle velocity are calculated for each particle by Eqs. (12), (11), and (10).
(3) The new positions and hosting cell of each particle are calculated by Eq. (8). First, the intersection of the flow vector and cell side is searched for by Eq. (13), and then the position of each particle is calculated by Eq. (15) if they are on the side or have a positive remaining distances. If the cell side that is located is a reflective boundary, the new particle position is modified by Eq. (16) and repeat step (3).
(4) If the remaining distance is positive, then the particle is still the cell k, and repeat from step (2). If negative, the particle is outside the k cell. Select the adjacent cell sharing the side with cell k and maximizing the Eq. (13). If the cell is in the HVT area, then increase the number of particles entering the HVT and return to step (3).

The maximum time step size Δt_p in Eq. (10) should be small enough to keep the traced particle position within the solution domain for the cases of low particle density and small particle diameter and especially at the region with an instantaneous change of fluid velocity.

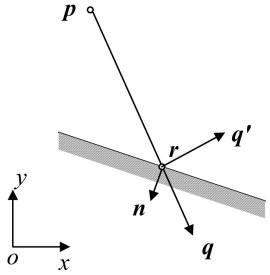

Fig. 3. Treatment of Reflective Boundary

3. CALCULATION OF PARTICLE TRANSPORT

3.1 Calculation Domain and Hydraulic Calculation

The method described above was applied to the debris transport problem on the containment floor following a large break LOCA of APR1400. Fig. 4 shows a computational domain of APR1400 containment. The domain is composed of an annulus region between the containment inner wall (CIW) and four pieces of the secondary shield wall (SSW), two D-shaped regions between the SSW and primary shield wall (PSW) excluding two steam generator (SG) pedestals and four reactor coolant pump (RCP) pedestals. On the right-hand side of the domain, the Hold-up Volume Tank (HVT) was surrounded by three pieces of HVT shield structures (HSS) allowing four entrances to HVT. On the left, the structural walls of the compartment for the letdown heat exchanger and the wall for the reactor drain tank are boundaries for the domain.

The solution domain was discretized by unstructured triangular meshes. Fig. 4 also shows the mesh distribution. The number of cells and nodes were 7228 and 4245, respectively. The discretization of the solution domain significantly improved from the one used in the author's previous calculation [8]. The major improvements were the reduction of the difference between sizes of meshes, i.e., more homogeneous mesh distribution, and the introduction of the compartment structures on the left-hand-side of the domain, which resulted in an increase in the number of meshes. It is expected that reliable calculation results can be obtained by those improvements. The present SWE solver was already justified by the comparison with experimental data in [8].

A hot leg double ended guillotine break LOCA of the APR1400 was assumed and the break flow rate was

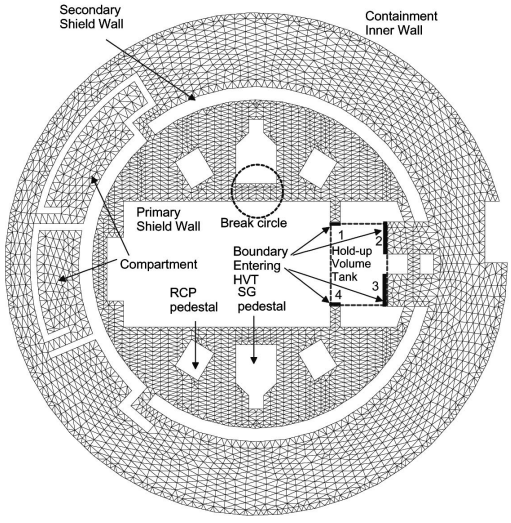

Fig. 4. Calculation Domain and Meshes for APR1400 Containment

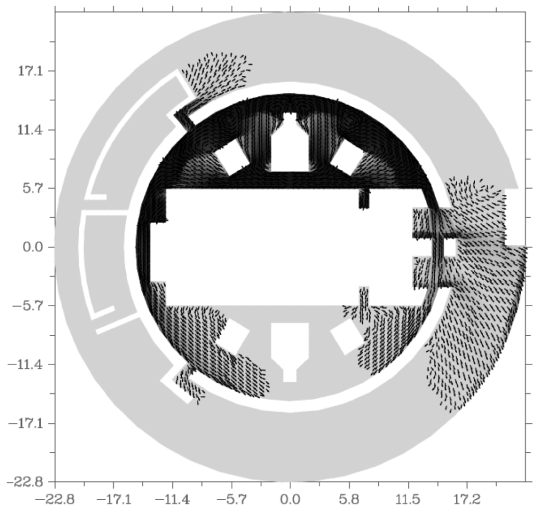

(a) t=5 sec

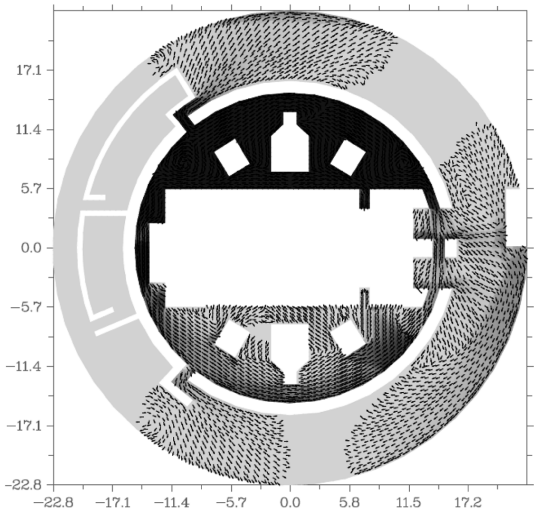

(b) t=10 sec

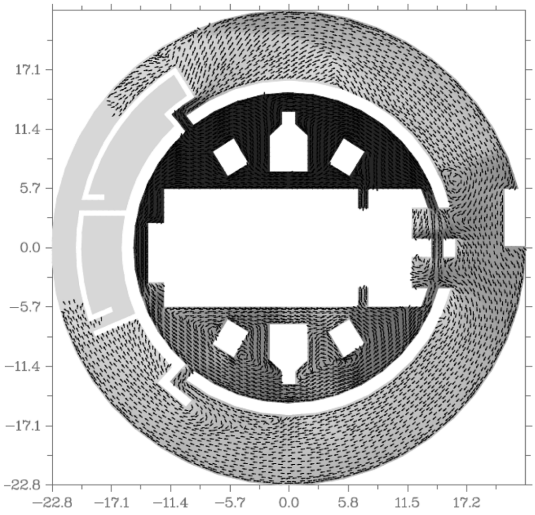

(b) t=30 sec

Fig. 5. Result of Flow Field Calculation

adopted as a function of time from the safety analysis report (SAR) [6]. Detailed description is available in the reference [8]. The calculation was conducted for 200 seconds.

Fig. 5 shows the calculated water level distribution and velocity vectors over the domain at 5, 10, and 30 seconds after LOCA, respectively. The region without a velocity vector can be regarded as a dry floor. From the comparison between three figures, water spreading behavior and the related wave propagation both inside and outside SSW can be observed.

3.2 Particle Tracking Calculation

3.2.1 Base Calculation

For the particle tracking, a calculation was conducted for the particle whose diameter and density were 0.02 m and 900 kg/m^3, respectively. The particles were assumed to initially be within a circle whose center and radius are (0, 6.5151 m) and 0.9 m, respectively (a region between PSW and the SG pedestal in the upper D-shaped area) and they were randomly distributed within the circle. The particles were added to the circle such that the number of particles decreased linearly from 98 at zero seconds to 2 at 9.5 seconds, as shown in Fig. 6. In total, 1000 particles were traced. The reason for the assumption was that behavior of the debris generation was similar to the behavior of the break flow. It was found from the sensitivity study that the instantaneous addition of debris particles at zero seconds led to a non-conservative result in the viewpoint of the number of particles entering the HVT due to the initially high fluid velocity, which expelled the particles far from the HVT entrance 1 where the most particles are trespassing. The calculation time step was 0.001~0.01 seconds which was selected for the given velocity field. The validity of the present particle tracking model was not fully addressed in this paper; however, it is believed that the accuracy of the particle tracking is strongly

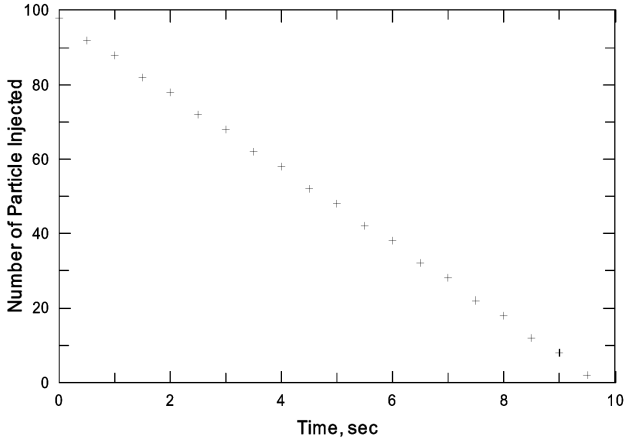

Fig. 6. Variation of Number of Particles Injected

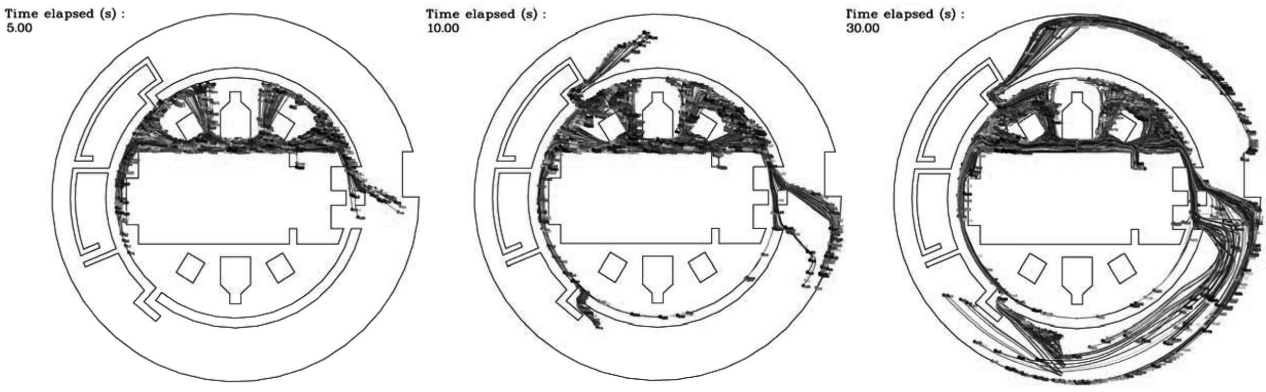

(a) t=5 sec (b) t=10 sec (c) t=30 sec

Fig. 7. Result of Debris Particle Tracking

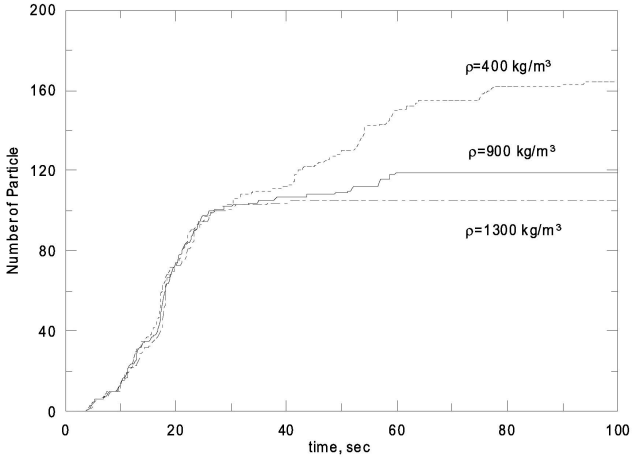

Fig. 8. Comparison of the Number of Particles Entering HVT (Effect of Density)

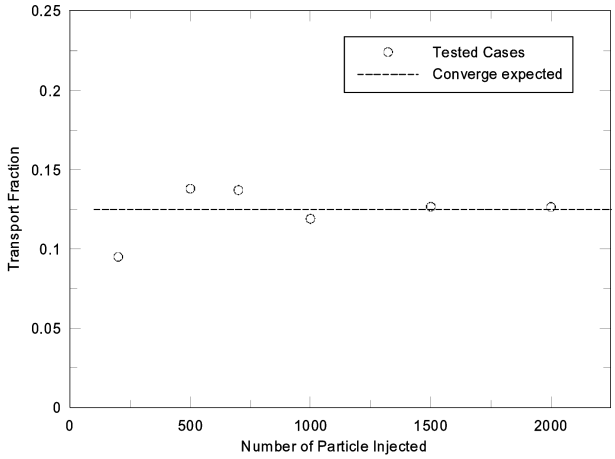

Fig. 9. Convergence of Transport Fraction with Number of Particles

dependent on the accuracy of the velocity field used.

Figs. 7(a), (b), and (c) show the calculated particle trajectories at 5, 10, and 30 seconds. Comparing the three figures indicates that a large number of particles existed on the containment floor for 10 seconds and a few particle trajectories were run to HVT. The reason for few particles entering the HVT before 10 seconds was the high velocities of the particles near entrance 1. As time progressed, the particles with relatively low velocities were entrained by fluid flow to the HVT entrance 1. The velocities of the particles were still high near entrances 2 and 3, which was due to acceleration through the narrow passage between HSS and SSW. Fig. 8 shows the number of particles entering HVT with respect to time. The number of particle significantly increased from 10 seconds onwards. For the case of density 900 kg/m^3, 120 among 1000 particles were transported to HVT until 100 seconds. From the results at 100 seconds, it is believed that, without a settling mechanism, some of the debris may remain at a certain local region of the containment floor and not move to the HVT when considering the particle trajectories that were determined by flow field, drag force, and geometrical effect. As in the calculation results, an almost steady state flow field was established at 100 seconds. At this time, there was a negligible flow from the region outside the secondary shield wall (annulus region) to the region inside. It is clear that the debris that was transported to the annulus region early will not be returned to the inside region. As a result, TF will be less than one.

3.2.2 Convergence Test

The calculated TF above was preliminary because it was not certain whether or not the TF from the 1000 particles was sufficiently reliable since random distribution was assumed. For this aspect, additional calculations were conducted to confirm the convergence of the calculated TF by changing the total number of particles added. Fig. 9 shows the results from those convergence calculations. As shown in the figure, the convergence can be guaranteed by increasing the total number of particles, and the TF

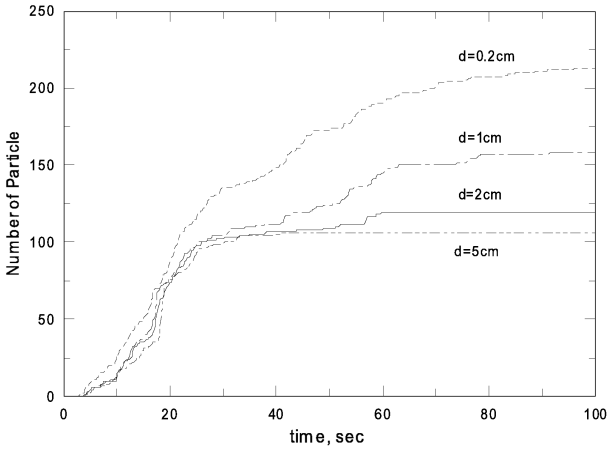

Fig. 10. Comparison of the Number of Particles Entering HVT (Effect of Size)

calculated from 1000 particles can be credited up to 10^{-2} level (0.12 at 1000 particles vs. 0.126 at 2000 particles).

3.2.3 Effect of Particle Density

A particle density of 900 kg/m^3 was used in the base calculation. The debris of low density fiber glass may be included following a LOCA. To understand the effect of particle density on transport, additional calculations were conducted for particle densities of 400 and 1300 kg/cm^3 having a size of 0.02 m. Fig. 8 also compares the result of the sensitivity calculation with the base calculation. The result clearly shows the lower particle density resulted in an increase of particles entering to the HVT. The calculated TF was 0.164 for the case of 400 kg/cm^3. One can find the effect of lower density was noticeable after 30 seconds. The increase of particles to HVT after 30 seconds was due to the particles transported to entrance 3.

3.2.4 Effect of Particle Size

The particle diameter of 0.02 m was assumed in the base calculation. Generally, the spectrum of debris size may be variable. To understand the effect of particle size on transport, additional calculations were conducted for several particle sizes of 0.002, 0.01, and 0.05 m having a density of 900 kg/cm^3. Fig. 10 shows the comparison of the number of particles to reach the HVT for those cases. The comparison shows a clear trend that the smaller the particle size leads the more particles transported to the HVT. The calculated TF was 0.213 for the 0.002 m case. The reason for this trend was clearly due to the change of drag force to the particles with respect to the particle size.

4. CONCLUDING REMARKS

An analysis model on debris transport in the containment floor was developed in which the flow field was calculated by the Eulerian conservation equations of mass and momentum, and the debris particle was traced by the Lagrangean equation of motion using the flow field data. For the flow field calculation, two-dimensional Shallow Water Equation was solved using the Finite Volume Method, and the Harten-Lax-van Leer scheme was adopted in for the accuracy to capture the dry-to-wet interface. For the debris tracing, a simplified two-dimensional Lagrangean particle tracking model including drag force was developed. To find the positions of particles over the containment floor and to determine the positions of particles reflected from the solid wall, Martin's scheme and Haselbacher's scheme were used, respectively. The present model was applied to calculate the transport fraction to Hold-up Volume Tank, which is a unique flow path to the containment sump in APR1400. In conclusion, the debris transport through the containment floor to HVT following a LOCA can be predicted by the present model, and the effect of particle density and size on transport can be identified. The predicted transport fraction was preliminarily 13~22% for the particle density range of 400-1300 kg/m^3 and for the particle diameter range of 0.002-0.05 m. To improve the accuracy and reliability of the evaluation, further studies on validation of particle tracking model and debris addition scheme are required.

NOMENCLATURE

A	area
$B(t)$	added water mass in Eq.(1)
C	closed path surrounding A
$\boldsymbol{C}$	vector to centroid of a side
C_D	Drag coefficient
D_i	Drag force
d_i	diameter of particle
$\boldsymbol{F}, \boldsymbol{G}$	convective flux vector
g	gravitational acceleration
h	water level
$\boldsymbol{m_i}$	vector to centroid of three sides of triangle
$\boldsymbol{n_i}$	outward unit normal vector of three sides of triangle
n_m	Manning friction coefficient
n_x, n_y	x and y components of unit normal vector
$\boldsymbol{p}, \boldsymbol{q}$	successive position vectors of a particle
$\boldsymbol{q'}$	vector for modified position from reflective boundary
$\boldsymbol{R_x}, \boldsymbol{R_y}$	diffusive flux vector
$\boldsymbol{r}$	vector for intersection with side
$\boldsymbol{S}$	source term vector
s	wave speed
t	time
$\boldsymbol{t}$	unit vector from $\boldsymbol{p}$ to $\boldsymbol{q}$
$\boldsymbol{U}$	variable vector
$\boldsymbol{V}, \boldsymbol{V_f}$	fluid velocity vector
u, v	x, y component of fluid velocity
u_f, v_f	x, y component of fluid velocity

$\boldsymbol{x}_i$ particle position vector
$\boldsymbol{w}_i$ particle velocity vector
z_b bed elevation
Δt time step size in hydraulic calculation
Δt_p time step size in hydraulic calculation

Subscript

e effective
f friction, fluid
i particle
i, j, k index of node, side, cell
L, R left and right
o bed slope
m Manning
x, y, z rectangular coordinates

Superscript

HLL Harten-Lax-van Leer
n old time
$n+\frac{1}{2}$, intermediate time
n+1 new time
* intermediate state for wave speed in HLL scheme

Greeks

α multiplying coefficient
μ kinetic viscosity
v dynamic viscosity
ρ density

ABBREVIATION

APR Advance Power Reactor
CFD Computational Fluid Dynamics
CIW Containment Inner Wall
ECCS Emergency Core Cooling System
FVM Finite Volume Method
HLL Harten-Lax-van Leer
HSS Holdup Volume Tank Shield Structures
HVT Holdup Volume Tank
LOCA Loss-of-coolant Accident
PSW Primary Shield Wall
PWR Pressurized Water Reactors
RCP Reactor Coolant Pump
SG Steam Generator
SSW Secondary Shield Wall
SWE Shallow Water Equations
TF Transport Fraction

REFERENCES

[1] V. Rao, et al., "GSI-191 Technical Assessment: Parametric Evaluation for Pressurized Water Reactor Recirculation Sump Performance," NUREG/CR-6762, Los Alamos National Laboratory (2002).
[2] USNRC, "Results of Chemical Effects Head Loss Tests in a Simulated PWR Sump Pool Environment," Information Notice 2005-27, United States Nuclear Regulatory Commission (2005).
[3] S. W. Lee, et al., "Status and Future Plan on Performance Improvement of Recirculation Sump in Domestic Plants," 7th Nuclear Safety Analysis Symposium, KINS, Daecheon, Korea, June 25~26 (2009).
[4] V. Rao, et al., 2003, "Knowledge Base for the Effect of Debris on Pressurized Water Reactor Emergency Core Cooling Sump Performance," NUREG/CR-6808, United States Nuclear Regulatory Commission (2003).
[5] USNRC, Safety Evaluation by the Office of Nuclear Reactor Regulation Related to NRC Generic Letter 2004-02, Nuclear Energy Institute Guidance Report "Pressurized Water Reactor Sump Performance Evaluation Methodology," United States Nuclear Regulatory Commission (2004).
[6] KEPCO, Standard Safety Analysis Report APR-1400, Seoul, Korea. (1997).
[7] J. I. Lee, et al., "Debris Transport Analysis Related with GSI-191 in Advanced Pressurized Water Reactor Equipped with In-containment Refueling Water Storage Tank," Proceedings of Experiment and Computational Fluid Dynamics for Nuclear Reactor Safety (XCFD4NRS), Grenoble, France, Sep.10~12 (2008).
[8] Y. S. Bang, G.. S. Lee, B. G.. Huh, D. Y. Oh, and S. W. Woo, "Prediction of Free Surface Flow on Containment Floor Using Shallow Water Equation Solver," *Nucl. Eng. Technol.*, 41, 8 (2009).
[9] G. Gottardi and M. Venutelli, "Central Scheme for Two-Dimensional Dam-break Flow Simulation," *Advances in Water Resources*, **27** (2004).
[10] A. Harten, P.D. Lax, and B. van Leer, "On Upstream Differencing and Godunov-type Schemes for Hyperbolic Conservation Laws," *SIAM Review*, **25**, 1 (1983).
[11] Martin, G.D, et al., Particle Host Cell Determination in Unstructured Grids, *Computers and Fluids*, **38**, 101 (2009).
[12] Haselbacher, A., et al., An Efficient and Robust Particle-Localization Algorithm for Unstructured Grids, *Journal of Computational Physics*, **225**, 2198 (2007).
[13] Atsushi Ui, et al., "Development of a Numerical Method for Flooding Flow and Transport of LOCA-Generated Debris to Sump Screens," NTHAS5-I004, Proceedings of 5th Korea-Japan Symposium on Nuclear Thermal Hydraulics and Safety, Nov. (2006).
[14] E. Krepper, et al., "Numerical and Experimental Investigations for Insulation Particle Transport Phenomena in Water Flow," *Annals of Nuclear Energy*, **35**, 1564 (2008).
[15] Cain, S.A., Gartland, F., Johansson, A.E., "CFD Simulation of Debris Transport in a PWR Reactor Sump Following a Loss of Coolant Event," Proceeding of ASME International Mechanical Engineering Congress and Exposition, Orlando, Florida USA, IMECE2005-82912. (2005).